THE JOURNAL OF PHYSICAL CHEMISTRY Letters

Letter

pubs.acs.org/JPCL

Bulk Heterojunction versus Diffused Bilayer: The Role of Device Geometry in Solution p-Doped Polymer-Based Solar Cells

Anna Loiudice,[†,‡] Aurora Rizzo,*[,‡,§] Mariano Biasiucci,[⊥,#] and Giuseppe Gigli[†,‡,§]

[†]Dipartimento di Matematica e Fisica "Ennio De Giorgi", Università del Salento, via Arnesano, 73100 Lecce, Italy

[‡]CBN - Center for Biomolecular Nanotechnologies, Italian Institute of Technology, Energy Platform, Via Barsanti sn -73010 Arnesano, Lecce, Italy

[§]NNL CNR-Istituto Nanoscienze, c/o Distretto Tecnologico, via per Arnesano km.5, 73100 Lecce, Italy

[⊥]NNL-CNR Istituto di Nanoscienze, c/o Dip. Fisica Ed. G. Marconi, La Sapienza University, Roma, Italy

[#]Center for Life NanoScience@LaSapienza, Italian Institute of Technology, Viale Regina Elena 295, Roma, Italy

Supporting Information

ABSTRACT: We exploit the effect of molecular p-type doping of P3HT in diffused bilayer (DB) polymer solar cells. In this alternative device geometry, the p-doping is accomplished in solution by blending the F_4-TCNQ with P3HT. The p-doping both increases the film conductivity and reduces the potential barrier at the interface with the electrode. This results in an excellent power conversion efficiency of 4.02%, which is an improvement of ~48% over the p-doped standard bulk heterojunction (BHJ) device. Combined V_{OC}–light intensity dependence measurements and Kelvin probe force microscopy reveal that the DB device configuration is particularly advantageous, if compared to the conventional BHJ, because it enables optimization of the donor and acceptor layers independently to minimize the effect of trapping and to fully exploit the improved transport properties.

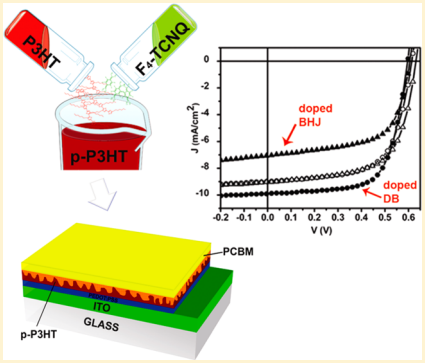

SECTION: Energy Conversion and Storage; Energy and Charge Transport

The control of the p- and n-type doping with well-defined levels of impurity represents one of the most successful strategies for the development of efficient both inorganic[1] and organic optoelectronic devices.[2−8] The addition of impurities with appropriate electronic properties leads to a shift of the Fermi level toward the transport states and to a reduction of the ohmic losses.[9] In the field of small-molecule-based devices, it has been demonstrated that the molecular doping can raise the conductivity by many order of magnitudes, well above the conductivity of pure materials.[10−13] This principle has been efficiently exploited in different kinds of optoelectronic devices, such as organic light-emitting diodes (OLEDs),[14] organic light-emitting field-effect transistors (OLEFETs),[15] and organic photovoltaic devices.[16,17]

Motivated by the success of the p-type doping concept in small-molecule devices, the interest in the doping of conjugated polymers has been recently manifested through experimental and theoretical studies on the system formed by the electron donor poly(3-exylthiophene) (P3HT) doped with tetrafluoro-tetracyanoquinodimethane (F_4-TCNQ), which is one of the strongest and widely used molecular electron acceptors.[18,19]

Although these reports have proven that upon doping, conductivity values increase up to 5 orders of magnitude over pristine P3HT,[19] the implementation of the doping technology in polymer solar cells remains still almost unexplored. Some attempts in this direction have been made by incorporating the strong electron acceptor, tetracyanoquinodimethane (TCNQ), in a standard BHJ device geometry. Such experiments have proven that the TCNQ acts as an electron trap if directly blended in the active layer, leading to enhanced recombination losses and to lower photovoltaic performances.[20] Given that the controlled doping in small-molecule devices relies on the ability to fabricate heterostructured stacks to correctly position the doped layers,[21] the difficulty to built multilayers by solution processing hinders the development of the doping concept in polymer devices.

In this Letter, we report improved power conversion efficiency (PCE) by solution-based p-type doping of the donor species in polymer solar cells. To efficiently exploit the doping effect, we propose an alternative device fabrication strategy, which consists of a sequential coating of the donor (i.e., P3HT) and acceptor (i.e., [6,6]-phenyl-C_{61}-butyric acid methyl ester, PCBM) species from orthogonal solvents and results in a DB device. The doping of P3HT with the strong electron acceptor, F_4-TCNQ, occurs via solution coblending prior the deposition. We demonstrate that the DB device configuration is particularly advantageous because it enables

Received: June 12, 2012
Accepted: July 3, 2012
Published: July 9, 2012

optimization of the donor and acceptor layers independently to minimize the effect of trapping and to fully exploit the improved transport properties of p-doped P3HT. The light doping (0.5% w/w dopant to polymer ratio) of the P3HT with F_4-TCNQ in the DB device leads to a greatly enhanced PCE of ~4.0%, compared to ~2.7% for the equally doped standard BHJ, which is an improvement of ~48%. The V_{OC}–light intensity dependence measurement shows that the trap-assisted recombination losses are not influenced by the p-type doping in the DB configuration, whereas they dramatically increase in the doped BHJ devices.

The fabrication process and the structure of our DB devices along with the energy level alignment and the chemical structures of the dopant (F_4-TCNQ), donor (P3HT), and acceptor (PCBM) materials are sketched in Figure 1a,b. The p-type doping of P3HT is accomplished by blending an appropriate quantity of F_4-TCNQ solutions with P3HT to achieve the desired w/w doping ratios. The device is made by sequential deposition of the P3HT, doped or pristine, from chlorobenzene and PCBM from dichloromethane, which leads to the formation of a DB device stack.[22,23] According to previously reported X-ray absorption near-edge structure (XANES) experiments, the doping of P3HT with F_4-TCNQ occurs via electron transfer from the highest occupied molecular orbital (HOMO) level of the P3HT to the lowest unoccupied molecular orbital (LUMO) level of the strong electron acceptor F_4-TCNQ (see the energy level alignment sketch in Figure 1b).[18] This leads to the formation of a ground-state charge-transfer complex and to a gradual shift of the P3HT Fermi level toward the HOMO. The p-doping both increases the film conductivity and reduces the potential barrier at the interface with the electrode. These findings were corroborated by subsequent studies on conductivity, UV–vis, Raman, and Fourier transform infrared (FTIR) analyses on different polymer/p-dopant systems.[19,24]

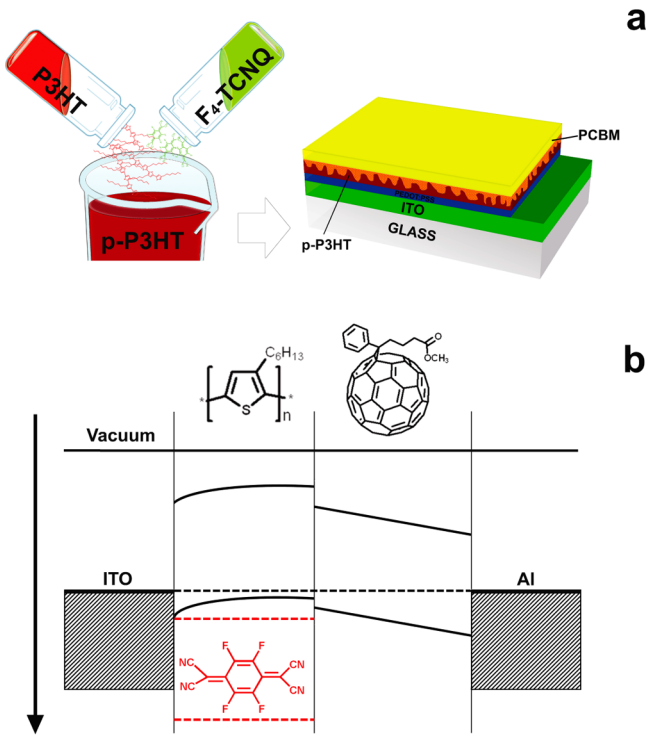

Figure 1. (a) A schematic representation of the solution preparation for the p-type layer to fabricate the doped diffused bilayer with F_4-TCNQ. (b) An energy diagram sketch to show the levels of the used donor, dopant, and acceptor.

To demonstrate that the p-doping approach is successfully applied to our DB whereas it is detrimental for the standard BHJ architecture, we test photovoltaic DB and BHJ devices with different percentages of F_4-TCNQ (0, 0.2, 0.5, 1, and 3% w/w). In Figure 2a and b, we compare the current density–voltage (J–V) curves in the dark and under illumination for the DB and BHJ devices at 0 and 0.5% doping percentage (see Figure S1 in the Supporting Information (SI) for J–V characteristics in the dark and under illumination for all of the doping percentages). Figure 2c–f and Table 1 present a summary of operating characteristics for all of the doping percentages in both DB and BHJ geometries. It can be readily observed that the 0.5% p-doping in the DB configuration leads to a considerable improvement in the J_{SC} and fill factor (FF) (the FF significantly increases from 63 to 68%, and the J_{SC} also increases from 8.96 to 9.89 mA·cm^{-2}), while these parameters drop drastically in the BHJ. The PCE for the 0.5% p-DB is as high as 4.02%, which is an overall 48% improvement over the equivalent p-BHJ device. It is noteworthy that the light doping for all of the percentages (0.2, 0.5, and 1%) in the DB geometry leads to higher PCE compared to that for the pristine DB as well. Overall, the PCE is improved from 3.45 to 4.02%, while the p-doping for BHJ devices results in a gradual reduction of the PCE from 3.57 to 1.37% by increasing the doping percentages (Table 1). The R_s and R_{sh} resistances for all of the devices are calculated from the inverse slope of the J–V dark characteristics at 0 V and at V_{OC}, respectively, and are schematized in Table 1.

In the DB configuration, the R_{sh} is increased by more than 1 order of magnitude for all of the dopant percentages, and the R_s is reduced for the light doping (0.2 and 0.5%). The improved resistances are strongly correlated to the FF values. Indeed, the higher FF can be associated with both the larger R_{sh}, which is related to fewer leakage currents, and the very low R_s, which increases the forward current and accounts for all of the resistances in the device (i.e., resistances to the interface transfer and transport in the film and through the contacts). In details, for the 0.5% light doping, the R_s value of 9.64 Ω·cm^2 is consistent with the ohmic behavior observed for the p-doped small-molecule-based solar cells.[21] The more ohmic-like contact for hole-injection at the PEDOT:PSS-p-doped P3HT interface, compared with that for the pristine P3HT, was also reported in "hole-only" devices.[19]

The higher FF can be also attributed to the improved selective transport of holes induced by the p-type doping of P3HT, which leads to a better rectification ratio (i.e., the ratio between the dark current at a fixed positive voltage value and the dark current at the same negative voltage value). We observed that the rectification ratio for the 0.5% DB calculated at +1 and −1 V is about 2 orders of magnitude larger than that of the pristine DB device (see SI, Figure S2). Moreover, a slight decrease of the V_{OC} values can be noted as the percentages of doping increase (Figure 2c). This trend can be attributed to the gradual raise of the P3HT HOMO level upon doping, which determines a reduction in the difference between the LUMO of the PCBM and the HOMO of P3HT.[25] Nonetheless, the reduction of the V_{OC} is compensated for by the positive effect of the light p-doping on the other photovoltaic parameters and PCE.

dx.doi.org/10.1021/jz300754p | J. Phys. Chem. Lett. 2012, 3, 1908–1915

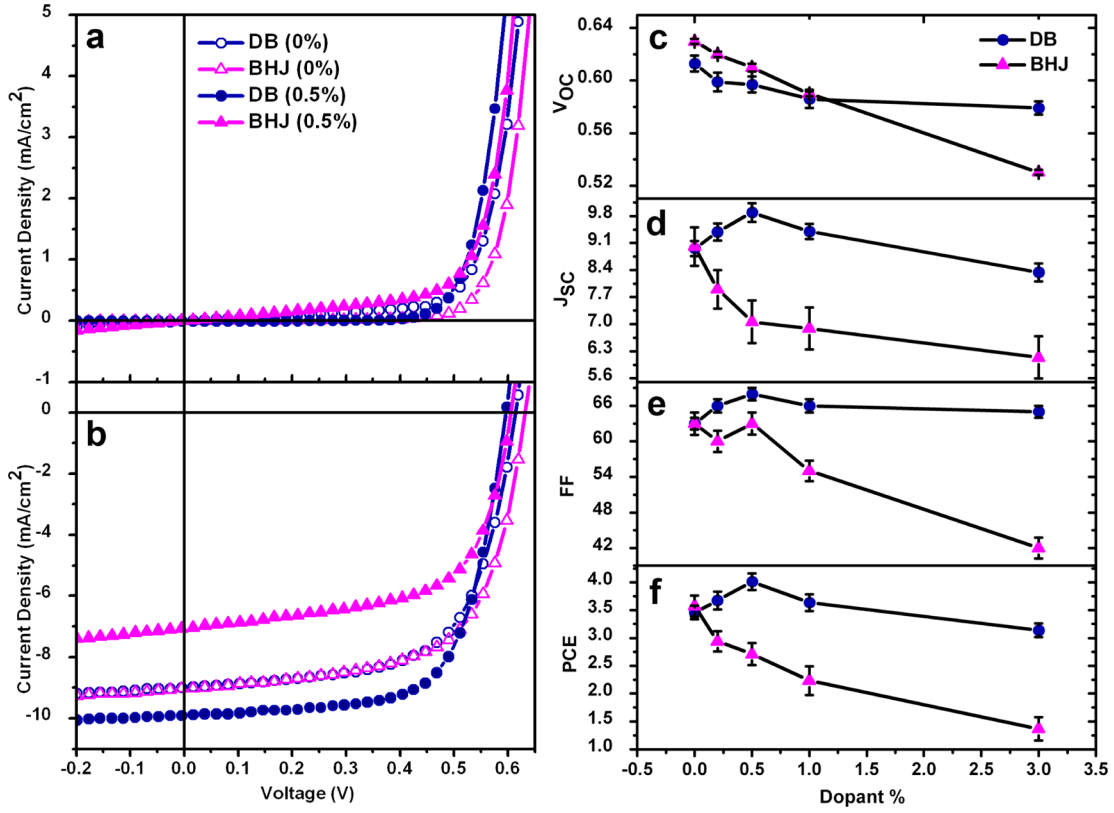

Figure 2. The current density of the DB and BHJ devices versus applied bias for the most meaningful dopant % in the dark (a) and under illumination (b), sharing the same legend: DB 0% (blue open circle), BHJ 0% (magenta open triangle), DB 0.5% (blue solid circle), and BHJ 0.5%. (magenta solid triangle). Panels (c–f) summarize the development of V_{OC}, J_{SC}, FF, and PCE as functions of the percentage of dopant for DB and BHJ devices. The error bars are calculated as the standard deviation from the mean value for a set of 15 devices.

Table 1. Performance of DB and BHJ Devices with Different Dopant % under 1.5 A.M Irradiation

dopant [%]	device structure	PCE [%]	FF	V_{OC} [V]	J_{SC} [mA·cm^{-2}]	R_{sh} [Ω·cm^2]	R_s [Ω·cm^2]
pristine-P3HT (0%)	DB	3.45	0.63	0.61	8.96	0.24×10^4	12.81
p-P3HT (0.2%)	DB	3.67	0.66	0.60	9.39	0.50×10^5	10.48
p-P3HT (0.5%)	DB	4.02	0.68	0.60	9.89	0.17×10^6	9.64
p-P3HT (1%)	DB	3.63	0.66	0.59	9.40	0.27×10^6	15.89
p-P3HT (3%)	DB	3.14	0.65	0.58	8.34	0.26×10^6	16.15
pristine-blend (0%)	BHJ	3.57	0.63	0.63	9.01	0.23×10^5	14.34
p-blend (0.2%)	BHJ	3.04	0.60	0.62	7.90	0.12×10^4	13.59
p-blend (0.5%)	BHJ	2.71	0.63	0.61	7.06	0.17×10^4	12.20
p-blend (1%)	BHJ	2.24	0.55	0.59	6.89	0.43×10^3	16.20
p-blend (3%)	BHJ	1.37	0.42	0.53	6.14	0.24×10^3	21.40

In contrast, in the BHJ configuration, the p-doping has a detrimental effect, which can be explained by the charge trapping phenomenon. We believe that in the BHJ rather than in the DB devices, the strong electron acceptor F_4-TCNQ sites act as electron traps, leading to substantial trap-assisted recombination losses that add to the bimolecular recombination. Indeed, in the BHJ active layer, the presence of traps at the interface between doped P3HT and PCBM is very likely because of the intimate intermixing of the two materials. In this case, upon the dissociation of the exciton at the P3HT/PCBM interface, part of the free electrons can be trapped and recombine with free holes in the acceptor, resulting in the loss of both carriers.[21]

To verify our hypothesis, that is, that the F_4-TCNQ acts as a trap in BHJ geometry whereas it does not in the DB, we investigate the light intensity dependence of the V_{OC}. In polymer photovoltaic devices, the extent of the trap-assisted recombination can be determined from the slope of V_{OC} versus the natural logarithm of the light intensity curves.[20,26] Indeed, at the higher trap density, that is, the stronger trap-limited recombination, the V_{OC}–light dependence is more enhanced. In Figure 3a,b, we show the dependence of the V_{OC} on the light intensity measured at different percentages of doping for the DB and BHJ geometries.

For polymer solar cells in the bimolecular Langevin recombination regime, we expect a linear trend with a slope proportional to the thermal voltage $kT{\cdot}q^{-1}$(k is Boltzmann's constant, T is the absolute temperature, and q is the electronic charge).[20] In the ideal case of absence of trapping phenomena, the slope of the linear fit should be just $kT{\cdot}q^{-1}$; the more the slope differs from the ideal value, the stronger the trap-limited recombination. The experimental data for the pristine DB

dx.doi.org/10.1021/jz300754p | J. Phys. Chem. Lett. 2012, 3, 1908–1915

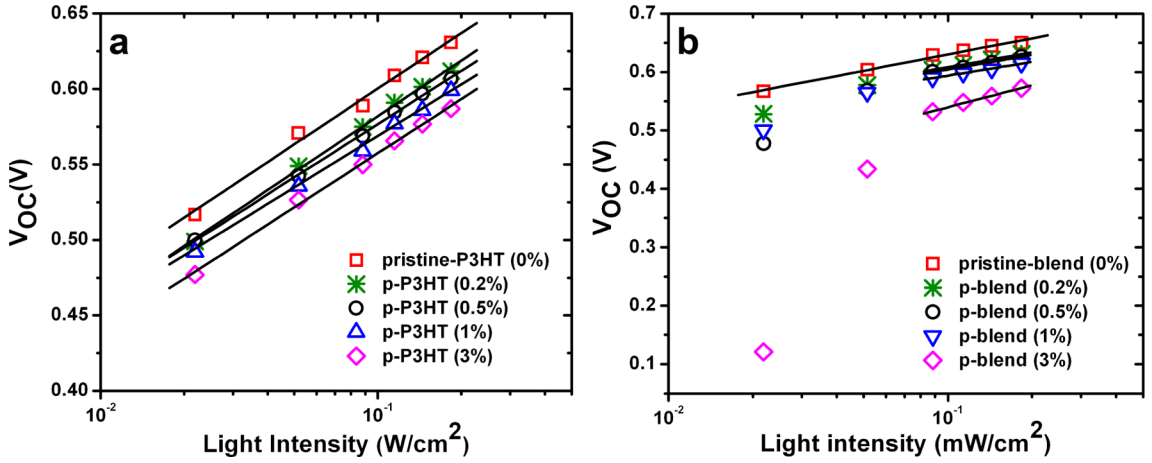

Figure 3. Open-circuit voltage of DB (a) and of BHJ (b) device structures as a function of the incident light power and for different dopant percentages: 0 (red squares), 0.2 (green asterisk), 0.5 (black circle), 1 (blue triangles), and 3% (magenta diamonds). The lines represent the linear fit to the experimental data.

device (Figure 3a) show a linear trend with a slope of $\sim 1.5kT \cdot q^{-1}$, indicating a nearly trap-free condition. Furthermore, it can be readily noted that the slope of the linear fits remains unchanged as the percentage of doping increases. In contrast, in the case of BHJ devices (Figure 3b), as expected, the linear trend can be observed solely in the undoped blend, while for doped devices, only a limited linear portion can be detected at higher light intensity. At low light intensity, the curves become steeper proportionally to the doping ratio. This behavior can be justified if we consider that the effect of charge trapping on the V_{OC} value is more pronounced at low carrier density, that is, at low light intensity, where the trap-assisted recombination dominates over the Langevin one.[26] Consequently, the steeper decay of the V_{OC}, compared to that of the DB devices, is direct evidence that the p-doped BHJ behaves as a trap-limited solar cell. The V_{OC}–light dependence data agree well with the photovoltaic performance. Moreover, in the trap-limited solar cells, the additional recombination losses of free charge carriers lead to a lower FF[27] and to a considerable reduction of the photocurrent as the dopant ratio increases (see Table 1). The combination of these effects results in a significant reduction of the solar cell performance for doped BHJ of a factor of 1.2–2.6 for the dopant percentages used in this study. Such a reduction can be attributed to morphological variation of the P3HT upon doping. In the SI (Figure S3), we compare the AFM topography micrographs of the pristine and lightly doped (0.5%) P3HT with the heavier doped (1 and 3%) P3HT spin-casted onto ITO/PEDOT:PSS substrates, following the device preparation conditions. Overall, the p-doped films show a larger surface roughness, which increases with the percentage of doping, 3.3 nm at 0%, 9.4 nm at 0.5%, 13.8 nm at 1%, and 21.8 nm at 3%. This gradual increase of the surface roughness provides direct evidence that the doping (particularly at the higher one) modifies the P3HT morphology by forming larger aggregates. In general, the performances of the photovoltaic devices are strongly dependent on the morphology of the active layer,[28] and specifically, in the DB configuration, the morphology of the P3HT can influence the diffusion of the PCBM.[29,30] Indeed, the presence of bigger aggregates on the surface of the highly doped P3HT may inhibit the diffusion of PCBM and result in a less extended active area for charge separation. Such diffusion can be also controlled by varying the amorphous to crystalline ratio domains in the P3HT film.[29] To verify whether the p-doping induces some modifications in the molecular order of the P3HT, we measured the UV–vis absorption spectra of pristine and doped P3HT films (see SI Figure S4). As the dopant concentration increases, the 520 nm absorption peak of the P3HT film slightly shifts toward 530 nm, and the relative intensity of the shoulder at ~550 nm enhances gradually. The red shift of the absorption peak indicates that the p-doped P3HT is characterized by an increased conjugation length due to the higher crystalline order.[31] We can conclude that the introduction of very small amounts of dopant molecules can influence the orientation of the P3HT. This is in good agreement with previously reported X-ray diffraction measurements,[19] which showed that the addition of small amount of F_4-TCNQ in P3HT leads to a more crystalline film. Consequently, the lower PCE of the heavily doped DB solar cells can be attributed to the poorer diffusion of PCBM in higher-crystalline-quality p-doped P3HT; in fact, the PCBM is preferentially miscible and mobile in disordered/amorphous P3HT regions. Thus, it can be hypothesized that in the DB, the direct contact between the F_4-TCNQ and the PCBM is reduced because the diffusion of PCBM is restrained in highly crystalline F_4-TCNQ-rich P3HT regions. However, in order to verify our hypothesis, a deeper understanding of the PCBM diffusion will require a reconstruction of the inner film structure by means of scattering techniques, such as grazing incidence small-angle X-ray scattering (GISAXS) or X-ray reflectivity (XRR).[32]

The presence of ground-state charge transfer from P3HT to F_4-TCNQ molecules can be observed in the absorption spectra (SI Figure S4) as a subgap absorption in the infrared region. Such a charge-transfer state is initiated by effective removal of electrons (oxidation) from polymers by electron-poor F_4-TCNQ molecules.[19] The subgap absorption is not seen in both P3HT and F_4-TCNQ films separately, and it is almost absent for light doping; however, it became detectable for a higher percentage of dopant.

In order to further demonstrate the existence of a p-doping effect also at a lower doping ratio, we perform electroluminescence (EL) measurement. By using EL, the detected luminescence signal can be made quite strong, and no pumping light is needed; therefore, scattering effects are completely avoided. The EL of devices containing 0, 0.2, 0.5, 1, and 3% was

dx.doi.org/10.1021/jz300754p | J. Phys. Chem. Lett. 2012, 3, 1908–1915

measured at +4 V, and the results are shown in Figure S5 in the SI. A significant EL quenching was observed even upon the addition of a small amount of F_4-TCNQ dopant. Such severe EL quenching indicates an efficient formation of free positive charges by addition of F_4-TCNQ molecules. These observations imply that the F_4-TCNQ molecules are well-dispersed within the polymer matrix.

To address the effect of molecular doping on the electrical conductivity of the P3HT film, we perform the conductive-AFM technique (C-AFM) in contact mode. For this purpose, we use a high work function metal Pt/Ir tip probe to measure thin films of pristine and p-doped P3HT on ITO substrates. Because the work functions of Pt/Ir and ITO are similar, the sandwich-type diode with bottom ITO and top Pt/Ir tip electrodes is a "hole-only" device, and in both directions of current flow, the hole injection barrier is smaller than the electron injection barrier. The conductivity values extrapolated from the plots in Figure 4 are listed in the table (inset).

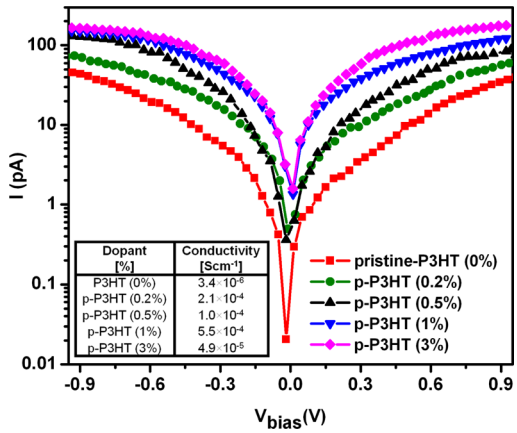

Figure 4. Current–electric field characteristics of P3HT hole-only devices, ITO/PEDOT:PSS/polymer (100 nm)/Pt, fabricated with pristine polymers and doped polymers with different amounts of F_4-TCNQ.

Notably, there is a significant improvement in conductivity even when a small quantity of molecular dopant is added to P3HT (i.e., 0.2%), and the maximum conductivity of 5.5×10^{-4} S cm^{-1} is reached at 1%, which is about 2 orders of magnitude improvement over that of the pristine P3HT. The reduction in conductivity of the heavily doped (3%) P3HT is in accordance with the decrease in the DB device performance.

To correlate the morphological and surface electronic properties of the device active layers, we perform Kelvin probe force microscopy (KPFM) measurements, which enable us to obtain surface photovoltage maps. The KPFM technique is performed by means of a noncontact AFM tip with a conductive coating and enables measurement of the difference between the tip potential and the local surface potential with a lateral resolution below 100 nm and a potential distribution of 10 mV. In addition, Kelvin probe measurement is a powerful tool for the investigation of the charge carrier generation and electron blocking effect at interlayers in polymer solar cells.[33]

We measure surface potential mapping of undoped and 0.5% doped DB and BHJ samples under different conditions (see Figure 5), before illumination (labeled "dark") and under illumination (labeled "light") with a white light source.

The surface potential curves (Figure 5b–e) are calculated from the $\Delta SP = \phi_{sample} - \phi_{tip}$.[34] The work function of the tip is measured by calibrating the cantilever on a highly oriented pyrolytic graphite (HOPG) reference sample; we obtain a work function of $\phi_{tip} = 5.25 \pm 0.02$ eV, which is consistent with values reported in the literature for PtIr-coated cantilevers.[35] In our experiment, the difference between the work functions of the tip and ITO electrode is estimated to be $\phi_{Ito} - \phi_{Tip} \approx -0.65$ eV by assuming $\phi_{Ito} \approx 4.6$ eV.[36]

Before illumination (dark, Figure 5a) the surface potential images for all of the samples (DB 0%, DB 0.5%, BHJ 0%, and BHJ 0.5%) show darker and brighter regions. Such contrast is remarkable in the doped samples, whereas it is less evident in the undoped ones; this is in agreement with the absence of charges in the pristine undoped organic semiconductors, and it is further proof of the effectiveness of the molecular p-doping. Indeed, following the conclusions of previous reports,[37] we attribute the slight in-dark contrast between the undoped P3HT and PCBM to band bending of the donor–acceptor blend at the PEDOT:PSS interface.

Under illumination, free charges are photogenerated at the P3HT/PCBM heterojunction after dissociation of excitons. The formation of charges can be revealed by a shift of the surface potential ($\Delta SP_{light-dark}$) under illumination and in the dark; see Figure 5b–e. It can be noted that the $\Delta SP_{light-dark}$ in the BHJ is smaller than that in the DB geometry, and in the doped devices, this shift is smaller than that in the undoped due to the formation of a charged state already in the dark for the doped films. We cannot however distinguish between the donor and acceptor domains because the charge separation occurs not only at the interface between the macrophases but also within each macrophase due to fine-scale phase separation. Resolving potential differences due to this fine-phase separation is beyond the resolution of our KPFM set up.[34]

Moreover, the $\Delta SP_{light-dark}$, calculated from Figure 5b and c, for the DB 0% and DB 0.5% are 320 and 190 mV, respectively; this reduction of the shift upon p-doping can be correlated with the slight reduction in the V_{OC} for the doped DB device (see Figure 2c and Table 1).

Overall, the KPFM results show clear differences in the electronic work function of the four active layers, which is a further confirmation of the how the different geometry and molecular doping can influence the film properties.

In conclusion, we successfully demonstrate a highly efficient DB polymer solar cell by simply doping the donor layer in solution. The p-type doping of P3HT, accomplished by blending appropriate quantities of F_4-TCNQ solutions with P3HT prior to deposition, improves the transport properties of the polymer, leading to a considerable improvement in the PCE efficiency compared to that for the device made from pristine P3HT. The V_{OC}–light intensity dependence measurements demonstrate that the DB configuration is particularly advantageous if compared to the conventional BHJ because it avoids the direct contact of the strong electron acceptor F_4-TCNQ with the PCBM, minimizing the effect of trapping. Our approach allows one to fully exploit the improved transport properties of p-doped P3HT and holds a great potential in the field of polymer-based solar cells. In principle, our p-type doping method can be applied to various polymer materials and can open novel routes toward highly efficient, multistacked solution-processable devices.

■ EXPERIMENTAL METHODS

Device Preparation. P3HT (Rieke metals, >98% regioregular) and F_4-TCNQ (Aldrich) were dissolved in chlorobenzene (20

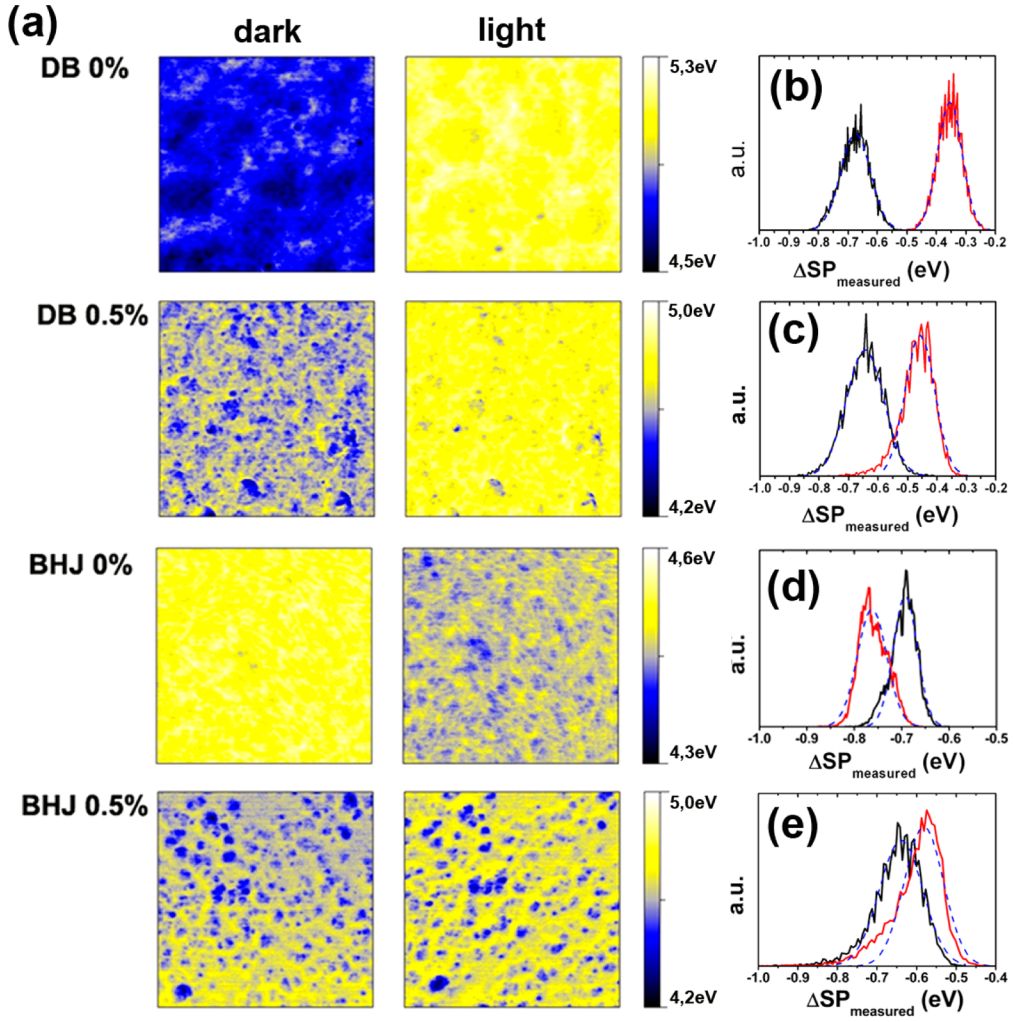

Figure 5. (a) Surface potential mappings of DB 0%, DB 0.5%, BHJ 0%, and BHJ 0.5% films on ITO/PEDOT:PSS in the dark and under light. The image sizes are 2 μm × 2 μm. On the right side are histogram distributions of the SP images (b–e). Black and red lines indicate dark and light measurements, respectively.

and 2 mg·mL^{-1}, respectively). Due to its limited solubility, stirring and heating of the F_4-TCNQ solutions up to 50 °C and filtering were required. For solutions, appropriate quantities of F_4-TCNQ solutions were added into the polymer solutions to achieve 0, 0.2, 0.5, 1, and 3% w/w (dopant to polymer weight ratio) doping concentrations. Immediately upon mixing, the color of the solution changed to black, while the pristine solutions were orange–red. $PC_{60}BM$ (NanoC) was dissolved in dichloromethane to produce a concentration of 5 mg·mL^{-1}. For the blend solutions, the previously prepared solutions of P3HT were added to the PCBM (blend ratio of 1:0.8) to obtain blend solutions at different doping concentrations. Photovoltaic solar cells were fabricated on ITO-coated glass substrates. The ITO-coated glass substrates were sequentially cleaned by ultrasonication in deionized water, acetone, and 2-propanol and then cleaned for 10 min at 85 °C using TL-1 solution cleaner. PEDOT:PSS (H. C. Stark, CLEVIOS) was spin-coated at 4000 rpm for 60 s to form a film of 40 nm thickness and dried at 140 °C for 15 min in nitrogen atmosphere. For the DB device, the P3HT (pristine or doped) solution was spin-coated onto the PEDOT:PSS layer at 1500 rpm for 60 s and was allowed to dry for 20 min. Then, the PCBM layer was spin-coated from dichloromethane at 4000 rpm for 10 s. The complete stack was annealed at 150 °C for 10 min. For the BHJ devices, the active layers were obtained by spin-coating the blend solution at 700 rpm for 45 s, followed by baking at 110 °C for 10 min. All of the device fabrication steps, except the spin-coating of PEDOT:PSS, were carried out in a glovebox under a controlled nitrogen atmosphere. Finally, to complete the device fabrication, the cathode (LiF ≈ 0.6 nm; Al ≈ 100 nm) was deposited through a shadow mask by thermal evaporation in a vacuum of about 6 × 10^{-6} Torr.

Device Characterization. The active area of the device has been accurately determined by an optical microscope, using a 4× magnification objective equipped with a ruler. Current density versus voltage (J–V) measurements were performed with an Air Mass 1.5 Global (AM 1.5 G) solar simulator with an irradiation intensity of 100 mW·cm^{-2}. V_{OC}–light dependence measurements were carried using a set of neutral filters. All of the measurements on the devices were conducted in glovebox under a controlled nitrogen atmosphere.

Morphological and Electrical Characterization. AFM imaging was carried out in air using a park scanning probe microscope (PSIA) operating in the tapping mode. The films for AFM investigations were prepared following the device fabrication procedure. The absorption measurements were recorded at room temperature with a Varian Cary 5000 UV–visible spectrometer. Devices for EL measurements were manufac-

dx.doi.org/10.1021/jz300754p | J. Phys. Chem. Lett. 2012, 3, 1908–1915

tured by spin films of pure or doped P3HT on ITO/PEDOT:PSS and after evaporating LiF/Al as the cathode. The EL spectra were performed at room temperature in air with encapsulation by using an OL-770 spectroradiometer (Optronic Laboratories). KPFM images were acquired with a commercial AFM system (Bruker-AXS) MultiMode AFM with a Nanoscope V controller operating in lift mode (typical lift height 20 nm) by using silicon tips with PtIr coating (SCM-PIT) with $k \approx 3\ \mathrm{N\ m^{-1}}$, tip radius ≈ 20 nm, and resonant frequency ≈ 80 Khz.

■ ASSOCIATED CONTENT

Supporting Information

Complete $I-V$ characterization of the devices in the dark and under illumination, AFM images, and absorption and electroluminescence measurements of P3HT films. This material is available free of charge via the Internet at http://pubs.acs.org.

■ AUTHOR INFORMATION

Corresponding Author

*E-mail: aurora.rizzo@nano.cnr.it. Tel. +39 0832 298211.

Notes

The authors declare no competing financial interest.

■ ACKNOWLEDGMENTS

This work was supported by the Italian projects Rete Nazionale di Ricerca sulle Nanoscienze ItalNanoNet (FIRB Reference Number RBPR05JH2P) and EFOR-Energia da FOnti Rinnovabili (Iniziativa CNR per il Mezzogiorno L. 191/2009 art. 2 comma 44) and by the European project ESCORT - Efficient Solar Cells based on Organic and hybrid Technology (seventh FWP, Reference Number 261920).

■ DEDICATION

Dedicated to the memory of Dr. Gianluca Latini, who passed away on March 2012.

■ REFERENCES

(1) Sze, S. M.; Ng, K. K. *Physics of Semiconductor Devices*, 3rd ed.; John Wiley & Sons, Inc.: Hoboken, NJ, 2007.

(2) Riede, M.; Mueller, T.; Tress, W.; Schueppel, R.; Leo, K. Small-Molecule Solar Cells — Status and Perspectives. *Nanotechnology* **2008**, *19*, 424001−424013.

(3) Blom, P. W. M.; Mihailetchi, V. D.; L. Koster, L. J. A.; Markov, D. E. Device Physics of Polymer:Fullerene Bulk Heterojunction Solar Cells. *Adv. Mater.* **2007**, *19*, 1551−1566.

(4) Christoph, J.; Brabec, C. J.; Gowrisanker, S.; Halls, J. J. M.; Laird, D.; Jia, S.; Williams, S. P. Polymer−Fullerene Bulk-Heterojunction Solar Cells. *Adv. Mater.* **2010**, *22*, 3839−3856.

(5) Helgesen, M.; Søndergaard, R.; Krebs, F. C. Advanced Materials and Processes for Polymer Solar Cell Devices. *J. Mater. Chem.* **2010**, *20*, 36−60.

(6) Ruderer, M. A.; Muller-Buschbaum, P. Morphology of Polymer-Based Bulk Heterojunction Films for Organic Photovoltaics. *Soft Matter* **2011**, *7*, 5482−5493.

(7) Günes, S.; Neugebauer, H.; Sariciftci, N. S. Conjugated Polymer-Based Organic Solar Cells. *Chem. Rev.* **2007**, *107*, 1324−1338.

(8) Xiaoniu Yang, X.; Loos, J. Toward High-Performance Polymer Solar Cells: The Importance of Morphology Control. *Macromolecules* **2007**, *40*, 1353−1362.

(9) Blochwitz, J.; Fritz, T.; Pfeiffer, M.; Leo, J. K.; Alloway, D. M.; Lee, P. A.; Amstrong, N. R. Interface Electronic Structure of Organic Semiconductors with Controlled Doping Levels. *Org. Electron.* **2001**, *2*, 97−104.

(10) Pfeiffer, M.; Beyer, A.; Fritz, T.; Leo, K. Controlled Doping of Phthalocyanine Layers by Cosublimation with Acceptor Molecules: A Systematic Seebeck and Conductivity Study. *Appl. Phys. Lett.* **1998**, *73*, 3202−3204.

(11) Nollau, A.; Pfeiffer, M.; Fritz, T.; Leo, K. Controlled n-Type Doping of a Molecular Organic Semiconductor: Naphthalenetetracarboxylic Dianhydride (NTCDA) Doped with Bis(ethylenedithio)-tetrathiafulvalene (BEDT-TTF). *J. Appl. Phys.* **2000**, *87*, 4340−4343.

(12) Maennig, B.; Pfeiffer, M.; Nollau, A.; Zhou, X.; Leo, K.; Simon, P. Controlled p-Type Doping of Polycrystalline and Amorphous Organic Layers: Self-Consistent Description of Conductivity and Field-Effect Mobility by a Microscopic Percolation Model. *Phys. Rev. B* **2001**, *64*, 195208−195217.

(13) Soeda, J.; Hirose, Y.; Yamagishi, M.; Nakao, A.; Uemura, T.; Nakayama, K.; Uno, M.; Nakazawa, Y.; Takimiya, K.; Takeya, J. Solution-Crystallized Organic Field-Effect Transistors with Charge-Acceptor Layers: High-Mobility and Low-Threshold-Voltage Operation in Air. *Adv. Mater.* **2011**, *23*, 3309−3314.

(14) Mazzeo, M; della Sala, F.; Mariano, F.; Melcarne, G.; D'Agostino, S.; Duan, Y.; Cingolani, R.; Gigli, G. Shaping White Light Through Electroluminescent Fully Organic Coupled Microcavities. *Adv. Mater.* **2010**, *22*, 4696−4700.

(15) Maiorano, V.; Bramanti, A.; Carallo, S.; Cingolani, R.; Gigli, G. Organic Light Emitting Field Effect Transistors Based on an Ambipolar p-i-n Layered Structure. *Appl. Phys. Lett.* **2010**, *96*, 133305−133308.

(16) Riede, M; Uhrich, C.; Widmer, J.; Timmreck, R.; Wynands, D.; Schwartz, G.; Gnehr, W.-M.; Hildebrandt, D.; Weiss, A.; Hwang, J.; Sundarraj, S.; Erk, P.; Pfeiffer, M.; Leo, K. Efficient Organic Tandem Solar Cells based on Small Molecules. *Adv. Funct. Mater.* **2011**, *21*, 3019−3028.

(17) Walzer, K.; Maennig, B.; Pfeiffer, M.; Leo, K. Highly Efficient Organic Devices Based on Electrically Doped Transport Layers. *Chem. Rev.* **2007**, *107*, 1233−1271.

(18) Aziz, E. F.; Vollmer, A.; Eisebitt, S.; Eberhardt, W.; Pingel, P.; Neher, D.; Koch, N. Localized Charge Transfer in a Molecularly Doped Conducting Polymer. *Adv. Mater.* **2007**, *19*, 3257−3260.

(19) Yim, K.-H.; Whiting, G. L.; Murphy, C. E.; Halls, J. J. M.; Burroughes, J. H.; Friend, R. H.; Kim, J.-S. Controlling Electrical Properties of Conjugated Polymers via a Solution-Based p-Type Doping. *Adv. Mater.* **2008**, *20*, 3319−3324.

(20) Mandoc, M. M.; Kooistra, F. B.; Hummelen, J. C.; de Boer, B.; Blom, P. W. M. Effect of Traps on the Performance of Bulk Heterojunction Organic Solar Cells. *Appl. Phys. Lett.* **2007**, *91*, 263505−263507.

(21) Drechsel, J.; Männig, B.; Gebeyehu, D.; Pfeiffer, M.; Leo, K.; Hoppe, H. MIP-Type Organic Solar Cells Incorporating Phthalocyanine/Fullerene Mixed Layers and Doped Wide-Gap Transport Layers. *Org. Electron.* **2004**, *5*, 175−186.

(22) Lee, K. H.; Schwenn, P. E.; Smith, A. R. G.; Cavaye, H.; Shaw, P. E.; James, M.; Krueger, K. B.; Gentle, I. R.; Meredith, P.; Burn, P. L. Morphology of All-Solution-Processed "Bilayer" Organic Solar Cells. *Adv. Mater.* **2011**, *23*, 766−770.

(23) Chen, C.; Liu, F.; Wang, C.; Nakahara, A.; Russell, T. P. Bulk Heterojunction Photovoltaic Active Layers via Bilayer Interdiffusion. *Nano Lett.* **2011**, *11*, 2071−2078.

(24) Deschler, F.; Da Como, E.; Limmer, T.; Tautz, R.; Godde, T.; Bayer, M.; von Hauff, E.; Yilmaz, S.; Allard, S.; Scherf, U; Feldmann, J. Reduced Charge Transfer Exciton Recombination in Organic Semiconductor Heterojunctions by Molecular Doping. *Phys. Rev. Lett.* **2011**, *107*, 127402−127404.

(25) Tress, W.; Leo, K.; Riede, M. Influence of Hole-Transport Layers and Donor Materials on Open-Circuit Voltage and Shape of $I-V$ Curves of Organic Solar Cells. *Adv. Funct. Mater.* **2011**, *21*, 2140−2149.

(26) Mandoc, M. M.; Veurman, W.; Koster, L. J. A.; de Boer, B.; M. Blom, P. W. Origin of the Reduced Fill Factor and Photocurrent in MDMO-PPV: PCNEPV All-Polymer Solar Cells. *Adv. Funct. Mater.* **2007**, *17*, 2167−2173.

(27) Koster, L. J. A.; Mihailetchi, V. D.; M. Blom, P. W. Bimolecular Recombination in Polymer/Fullerene Bulk Heterojunction Solar Cells. *Appl. Phys. Lett.* **2006**, *88*, 052104−052107.
(28) Chen, D.; Nakahara, A.; Wei, D.; Nordlund, D.; Russell, T. P. P3HT/PCBM Bulk Heterojunction Organic Photovoltaics: Correlating Efficiency and Morphology. *Nano Lett.* **2011**, *11*, 561−567.
(29) Loiudice, A.; Rizzo, A.; Latini, G.; Nobile, C.; De Giorgi, M.; Gigli, G. Graded Vertical Phase Separation of Donor/Acceptor Species for Polymer Solar Cells. *Sol. Energy Mater. Sol. Cells* **2012**, *100*, 147−152.
(30) Treat, N. D.; Brady, M. A.; Smith, G.; Toney, M. F.; Kramer, E. J.; Hawker, C. J.; Chabinyc, M. L. Interdiffusion of PCBM and P3HT Reveals Miscibility in a Photovoltaically Active Blend. *Adv. Energy Mater* **2011**, *1*, 82−89.
(31) Zen, A.; Saphiannikova, M.; Neher, D.; Asawapirom, U.; Scherf, U. Comparative Study of the Field-Effect Mobility of a Copolymer and a Binary Blend Based on Poly(3-alkylthiophene)s. *Chem. Mater.* **2005**, *17*, 781−786.
(32) Ruderer, M. A.; Guo, S.; Meier, R.; Chiang, H.-Y.; Körstgens, V.; Wiedersich, J.; Perlich, J.; Roth, S. V.; Müller-Buschbaum, P. Solvent-Induced Morphology in Polymer-Based Systems for Organic Photovoltaics. *Adv. Funct. Mater.* **2011**, *21*, 3382−3391.
(33) Hoppe, H.; Glatzel, T.; Niggmann, M.; Schwinger, W.; Shaeffer, F.; Hinsch, A.; Lux-Steiner, M. Ch.; Sariciftci, N. S. Efficiency Limiting Morphological Factors of MDMO-PPV: PCBM Plastic Solar Cells. *Thin Solid Film* **2006**, *511*, 587−592.
(34) Chiesa, M.; Bu1rgi, L.; Kim, Ji-S.; Shikler, R.; Friend, R. H.; Sirringhaus, H. Correlation between Surface Photovoltage and Blend Morphology in Polyfluorene-Based Photodiodes. *Nano Lett.* **2005**, *5*, 559−563.
(35) Grancini, G.; Biasiucci, M.; Mastria, R.; Scotognella, R.; Tassone, F.; Polli, D.; Gigli, G.; Lanzani, G. Dynamic Microscopy Study of Ultrafast Charge Transfer in Hybrid P3HT/Hyperbranched CdSe Nanoparticle Blend for Photovoltaics. *J. Phys. Chem. Lett.* **2012**, *3*, 517−523.
(36) Van Slyke, S. A.; Chen, C. H.; Tang, C. W. Organic Electroluminescent Devices with Improved Stability. *Appl. Phys. Lett.* **1996**, *69*, 2160−2162.
(37) Maturova, K.; Kemerink, M.; Wienk, M. M.; Charrier, D. S. H.; Janssen, R. A. J. Scanning Kelvin Probe Microscopy on Bulk Heterojunction Polymer Blends. *Adv. Funct. Mater.* **2009**, *19*, 1379−1386.